

Thermal aspects and particle dynamics of Euler-Heisenberg AdS black hole in 4D Einstein Gauss-Bonnet gravity

B. Hamil^a  Faisal Javed^{b,c}  *

^aLaboratoire de Physique Mathématique et Physique Subatomique, Faculté des Sciences Exactes, Université Constantine 1, Constantine, Algeria.

^bDepartment of Physics, Zhejiang Normal University, Jinhua 321004, People's Republic of China

^cResearch Center of Astrophysics and Cosmology, Khazar University, Baku, AZ1096, 41 Mehseti Street, Azerbaijan

February 24, 2026

Abstract

We construct charged AdS BH solutions in four-dimensional Einstein-GaussBonnet gravity coupled to EulerHeisenberg nonlinear electrodynamics and investigate their physical properties. The modified field equations admit black hole solutions whose horizon structure is significantly affected by higher-curvature and nonlinear electromagnetic corrections, allowing for multiple horizons depending on the model parameters. In the extended phase space, where the cosmological constant is interpreted as thermodynamic pressure, we analyze the thermodynamic behavior and show that both the GaussBonnet coupling and the EulerHeisenberg parameter induce notable modifications in the equation of state, critical behavior, and thermal stability. Interpreting the black hole mass as enthalpy, we study the Joule-Thomson expansion and determine the inversion temperature and pressure, demonstrating that higher-curvature and nonlinear electrodynamic effects substantially influence the cooling and heating regions. Finally, we examine timelike geodesics and show that GaussBonnet corrections significantly modify the effective potential, orbital stability, and particle motion in the strong-field regime.

Keywords: Black hole; Nonlinear electrodynamics; Modified theory; Thermodynamics.

1 Introduction

Nonlinear electromagnetic extensions of the Reissner-Nordström solution in EinsteinMaxwell theory have been extensively studied in recent years. A particularly important example is provided by the gravitating Born-Infeld (BI) theory [1]. Early studies of charged black holes (BHs) coupled to nonlinear electrodynamics (NLED) date back to the 1930s [2, 3]. Subsequent developments in string theory and D-brane physics revealed that Abelian and non-Abelian BI-type Lagrangians naturally emerge in the low-energy limit [4], thereby renewing interest in nonlinear electromagnetic actions. Within this framework, BH solutions of Einstein-Born-Infeld gravity were obtained in [5, 6].

*hamilbilel@gmail.com
faisaljaved.math@gmail.com

Nonlinear extensions of ReissnerNordström solutions in Einstein-Maxwell theory has drawn considerable attention while discussing the shortcomings of linear electrodynamics at the strong-field regime. Among these extensions, the gravitating Born-Infeld (BI) theory [1] is particularly interesting as BI has a strong physical motivation as he was the first to propose its application to regularizing the divergent self-energy of point charges. The study of static electrically charged BHs in the context of NLED goes back to the pioneering work of the 1930's [2, 3] in the absence of a BH where a horizon was understood. It was noted that the nonlinear correction may trigger a strong effect on the structure of the solutions' near horizon. With the progress of string theory and D-brane theory, it was possible to extend those theories and provide motivation for Abelian and non Abelian BI type Lagrangians [4] which substantially attracted attention on the nonlinear electromagnetic theory in gravity context. In the context of the aforementioned references, asymptotically flat static and spherically symmetric BH solutions of Einstein- Born-Infeld gravity [5, 6] were systematically studied and found to possess deviations from the Reissner Nordstrom geometry to non-Neilsian electrodynamics.

A variety of NLED models admitting static and spherically symmetric solutions have also been investigated over the past decades. These include models with Lagrangians given by general functions of the electromagnetic invariants $F_{\mu\nu}F^{\mu\nu}$ [7, 8], logarithmic modifications of the Maxwell invariant [9], and generalized nonlinear Lagrangians [10] that reproduce both the BI theory and the weak-field limit of the Euler-Heisenberg (EH) effective Lagrangian [11]. BH solutions arising from the coupling of gravity to NLED in the weak-field EH limit, interpreted as a low-energy approximation of the BI theory, were analyzed in [12]. Considerable effort has also been devoted to the construction of regular BHs in gravitating NLED [13–15], with their distinctive properties discussed in [16–31].

In the framework of Dirac's electronpositron theory, nonlinear electromagnetic fields were first modeled by Heisenberg and Euler [11]. Later, these non-perturbative one-loop effective Lagrangians were reformulated by Schwinger within the context of QED [32]. The effective theory obtained describes vacuum polarization, whose imaginary part corresponds to the vacuum decaying via electronpositron pair production. If the electric field value is above the critical value, which is given by $E_c = \frac{m^3 c^3}{e\hbar}$ the vacuum can be polarized by the spontaneous pair creation [11, 32]. For many years, a lot of theories and experiments have been oriented toward pair creation from QED vacuum and vacuum polarization due to external electromagnetic fields [33–39]. As a fundamental and experimentally well-tested theory, QED provides an accurate description of electromagnetic interactions, making the investigation of QED effects in BH physics particularly important. Consequently, the EH effective Lagrangian plays a central role in the construction and analysis of generalized BH solutions discussed above.

Lovelock theories [40, 41], which incorporate higher-order curvature terms, provide a natural generalization of Einstein's general relativity to higher-dimensional spacetimes, while preserving the second-order nature of the field equations (FEs) for the metric. So Lovelock gravity bypasses some challenges that are typical in other higher-derivative theories of gravity, where the equations of motion are of the fourth order or higher, and where linear perturbation analyses result in the emergence of ghost instabilities, among other things. More specifically, Einstein-Gauss-Bonnet (EGB) gravity, which is a second-order Lovelock theory, consists of a Lagrangian containing the Einstein-Hilbert term with a cosmological constant, and the quadratic Gauss-Bonnet (GB) term. EGB gravity has been the subject of a lot of research, in part because it is the low-energy effective theory of strings propagating in curved spacetime [42, 43]. In this context, BH solutions that are static and spherically symmetric were found by Boulware and Deser [44]. In 4-dimensions, the GB contribution is topological and does not modify the gravitational equations of motion in the absence of matter couplings. [45, 46].

More recently, a four-dimensional version of EGB gravity was introduced by Glavan and Lin [47] via a regularization scheme, in which the GB coupling α is rescaled as $\frac{\alpha}{D-4}$ in D dimensions and the limit $D \rightarrow 4$ is taken at the level of the NLED. It is worth noting that this regularization scheme has been the subject of ongoing debate, and several shortcomings have been pointed out in the literature [48–50]. Various proposals have been put forward to address these issues [51], yielding the same BH metric

as in the original formulation [47] and suggesting that it remains a valid solution. Consequently, the original regularization scheme may still be employed to investigate EGB gravity coupled to additional fields and to construct new BH solutions. Research on BHs in 4-dimensional EGB gravity has attracted considerable attention, and various aspects such as thermodynamics, quasinormal modes, BH shadows, and stellar structure have been extensively studied within this framework [52–70].

Four-dimensional EGB gravity provides an effective higher-curvature extension of general relativity that admits well-defined BH solutions while retaining second-order NLED. EH NLED, derived as the one-loop effective action of QED in the weak-field limit, introduces nonlinear electromagnetic corrections associated with vacuum polarization effects. Investigating BHs within this combined framework enables the assessment of the interplay between higher-curvature gravity and nonlinear electromagnetic fields, clarifying their impact on the structure and physical properties of BH spacetimes. This model allows for a detailed analysis of thermodynamic behavior and phase structure, including the Joule-Thomson (JT) expansion and the associated cooling and heating processes. Since both GB and EH corrections are expected to influence the equation of state and thermodynamic response, a joint analysis is required to understand their combined effects on cooling and heating processes. In addition, the examination of test particle motion offers complementary information on orbital stability and strong-field effects induced by these corrections. Motivated by these considerations, we analyze charged AdS BHs in D4 EGB gravity coupled to EH NLED, focusing on their thermodynamics, JT expansion, and geodesic structure.

This paper is structured as follows. Section 2 discusses the action of EGB gravity coupled to EH NLED. We derive the relevant NLED and BH solutions. In Sect. 3, we explore BH thermodynamics in the extended phase space: equations of state, critical phenomena, and thermal stability. Sect. 4 concerns the JT expansion, where we obtain inversion temperature and pressure and describe the relevant cooling and heating regions. In Sect. 5, we discuss the motion of test particles along geodesics, with an emphasis on the effective potential, circular orbits, epicyclic frequencies, and the innermost stable circular orbit (ISCO). Our conclusions are stated in Sect. 6.

2 Action, Field Equations and Solution

We consider EGB gravity in D -dimensions coupled to EH NLED. The dynamics of the system is governed by the action [71, 72],

$$\mathbf{S} = \frac{1}{16\pi} \int d^D x \sqrt{-g} \left[R - \frac{(D-1)(D-2)}{3} \Lambda - 4\mathcal{L}^{\text{EH}}(F, G) + \alpha\mathcal{L}^{\text{GB}} \right], \quad (1)$$

here we used cosmological constant (Λ), Ricci scalar (R), $g = (\det g_{\mu\nu})$, and α is the coupling constant. The GB Lagrangian \mathcal{L}^{GB} is defined as

$$\mathcal{L}^{\text{GB}} = R^2 - 4R_{ab}R^{ab} + R_{abcd}R^{abcd}, \quad (2)$$

with Riemann tensor (R_{abcd}) and Ricci tensor (R_{ab}). The EH Lagrangian $\mathcal{L}^{\text{EH}}(F, G)$ takes the form

$$\mathcal{L}^{\text{EH}}(F, G) = -F + \frac{a}{2}F^2 + \frac{7a}{8}G^2, \quad (3)$$

the electromagnetic invariants are given by

$$F = \frac{1}{4}F_{\mu\nu}F^{\mu\nu} \quad \text{and} \quad G = \frac{1}{4}F_{\mu\nu}^*F^{\mu\nu}, \quad (4)$$

here $F_{\mu\nu} = \partial_\mu A_\nu - \partial_\nu A_\mu$ is the usual Maxwell tensor. The parameter a controls the strength of EH NLED corrections. In order to simplify the NLED, we employ the Legendre-dual formulation of NLED

introduced by Plebański [71]. In this approach, one defines the tensor $P_{\mu\nu}$

$$P_{\mu\nu} = (1 - aF) F_{\mu\nu} - {}^*F_{\mu\nu} \frac{7a}{4} G, \quad (5)$$

which allows one to construct two independent scalar invariants expressed as

$$s = -\frac{1}{4} P_{\mu\nu} P^{\mu\nu} \quad \text{and} \quad t = -\frac{1}{4} P_{\mu\nu} {}^*P^{\mu\nu}. \quad (6)$$

To first order in the parameter a , the EulerHeisenberg Hamiltonian density takes the form

$$\mathcal{H} = s - \frac{a}{2} s^2 - \frac{7a}{8} t^2. \quad (7)$$

The equations of the gravitational field are obtained by varying the action (1) with respect to the metric.

$$R_{\mu\nu} - \frac{1}{2} g_{\mu\nu} R + \frac{(D-1)(D-2)}{3} \Lambda + \alpha H_{\mu\nu}^{\text{GB}} = T_{\mu\nu}^{\text{EH}}, \quad (8)$$

supplemented by the electromagnetic field equation

$$\nabla_{\mu} P^{\mu\nu} = 0.$$

Here $H_{\mu\nu}^{\text{(GB)}}$ is the Lanczos tensor [73]

$$H_{\mu\nu} = 2 \left(-R_{\mu c d \lambda} R_{\nu}^{d \lambda c} + R R_{\mu\nu} - 2R_{\mu\nu b c} R^{d c} - 2R_{\mu c} R_{\nu}^c \right) - \frac{1}{2} \mathcal{L}^{\text{GB}} g_{\mu\nu}, \quad (9)$$

while the stress-energy tensor of the EH field in the P framework is given by [72],

$$T_{\mu\nu}^{\text{EH}} = (1 - as) P_{\mu}^{\sigma} P_{\nu\sigma} + g_{\mu\nu} \left(s - \frac{3a}{2} s^2 - \frac{7a}{2} t^2 \right), \quad (10)$$

In the limit $a \rightarrow 0$, the standard Maxwell energy-momentum tensor is recovered. Now, we consider the line element as

$$ds^2 = -\mathcal{F}(r) dt^2 + \frac{1}{\mathcal{F}(r)} dr^2 + r^2 d\Omega_{D-2}^2, \quad (11)$$

where $(D-2)$ dimensional unit sphere is denoted by $d\Omega_{D-2}^2$. It can be expressed as

$$d\Omega_{D-2}^2 = d\theta_{D-3}^2 + \sin^2 \theta_{D-3} \left(d\theta_{D-4}^2 + \sin^2 \theta_{D-4} \left(\dots + \sin^2 \theta_2 \left(d\theta_1^2 + \sin^2 \theta_1^2 d\varphi \right) \right) \right). \quad (12)$$

For this ansatz, the (t,t) component takes the form

$$T_0^0 = \frac{D-2}{2} \left[\frac{\mathcal{F}(r)'}{r} + \frac{(D-3)\mathcal{F}(r)}{r^2} - \frac{D-3}{r^2} + \frac{(D-1)}{3} \Lambda \right] - \frac{\alpha(D-2)(D-3)(D-4)}{2} \times \left[\frac{2\mathcal{F}(r)\mathcal{F}(r)'}{r^3} - \frac{2\mathcal{F}(r)'}{r^3} + \frac{(D-5)\mathcal{F}(r)^2}{r^4} - \frac{2(D-5)\mathcal{F}(r)}{r^4} + \frac{(D-5)}{r^4} \right]. \quad (13)$$

It is interesting to mention that topologically GB term is referred as four dimensions, a nontrivial contribution can be obtained by adopting the regularization procedure proposed in [47]. Rescaling the coupling constant as $\alpha \rightarrow \alpha/(D-4)$ and taking the limit $D \rightarrow 4$, one finds

$$T_0^0 = \left[\frac{\mathcal{F}(r)'}{r} + \frac{\mathcal{F}(r)}{r^2} - \frac{1}{r^2} \right] + \Lambda - \alpha \left[\frac{2\mathcal{F}(r)\mathcal{F}(r)'}{r^3} - \frac{2\mathcal{F}(r)'}{r^3} - \frac{\mathcal{F}(r)^2}{r^4} + \frac{2\mathcal{F}(r)}{r^4} - \frac{1}{r^4} \right]. \quad (14)$$

We restrict attention to a purely electric configuration with charge Q . In this case, the only nonvanishing component of $P_{\mu\nu}$ is

$$P_{\mu\nu} = \frac{Q}{r^2} (\delta_\mu^0 \delta_\nu^1 - \delta_\mu^1 \delta_\nu^0), \quad (15)$$

which yields the electromagnetic invariants

$$s = \frac{Q^2}{2r^4} \quad \text{and} \quad t = 0. \quad (16)$$

by using $\mathcal{F}(r) = 1 + \mathcal{G}(r)$ the NLED reduce to

$$(r^3 - 2\alpha r \mathcal{G}(r)) \mathcal{G}(r)' + (r^2 + \alpha \mathcal{G}(r)) \mathcal{G}(r) + \Lambda r^4 + \frac{Q^2}{2} - \frac{aQ^4}{8r^4} = 0. \quad (17)$$

Upon integration, one obtains the metric function describing a 4D EGB black hole coupled to EH NLED

$$\mathcal{F}(r) = \frac{2\alpha + r^2}{2\alpha} \left(1 \pm \sqrt{1 + \frac{4\alpha}{r^2} \left(\frac{2M}{r} - \frac{Q^2}{r^2} + \frac{\Lambda}{3} r^2 + \frac{aQ^4}{20r^6} \right)} \right), \quad (18)$$

The solution in Eq. (18) follows from the dimensional regularization scheme introduced in [47] and is compatible with the consistent Aoki-Gorji-Mukohyama theory of 4D EGB gravity [74]. This class of BHs is parametrized by the mass M , cosmological constant Λ , EH NLED nonlinear parameter a , electric charge Q , and GB coupling constant α . For $a = 0$, Eq.(18) reduces to the BH solution previously obtained in [75]. In order to analyze the general structure of the solution (18), we consider the limit $\alpha \rightarrow 0$. For the branch corresponding to the minus sign " - ", the metric function becomes

$$\mathcal{F}(r) = 1 - \frac{2M}{r} + \frac{Q^2}{r^2} - \frac{\Lambda}{3} r^2 - \frac{aQ^4}{20r^6}, \quad (19)$$

which describes an asymptotically AdS BH coupled to EH NLED. In contrast, for the branch associated with the plus sign " + ", we have

$$\mathcal{F}(r) = 1 + \frac{2M}{r} - \frac{Q^2}{r^2} + \left(\frac{\Lambda}{3} + \frac{1}{\alpha} \right) r^2 + \frac{aQ^4}{20r^6}.$$

This branch effectively reduces to a charged-(A)dS type solution with negative gravitational mass and an imaginary electric charge, rendering it physically unacceptable. Consequently, the minus branch represents the physically meaningful solution. In what follows, we therefore restrict our analysis to the negative branch only. We now examine the horizon structure of the spacetime, which is determined by the condition

$$\mathcal{F}(r) = 1 + \frac{r^2}{2\alpha} \left(1 - \sqrt{1 + \frac{4\alpha}{r^2} \left(\frac{2M}{r} - \frac{Q^2}{r^2} + \frac{\Lambda}{3} r^2 + \frac{aQ^4}{20r^6} \right)} \right) = 0. \quad (20)$$

The roots of this equation determine the horizon structure of the BH. In general, the BH admits three positive real roots: the event horizon, r_+ , the inner (Cauchy) horizon, r_- , and the cosmological horizon, r_C . Figure 1 displays the behavior of the metric function $\mathcal{F}(r)$ for different values of the parameters α and a , which encode the effects of EGB gravity and NLED, respectively.

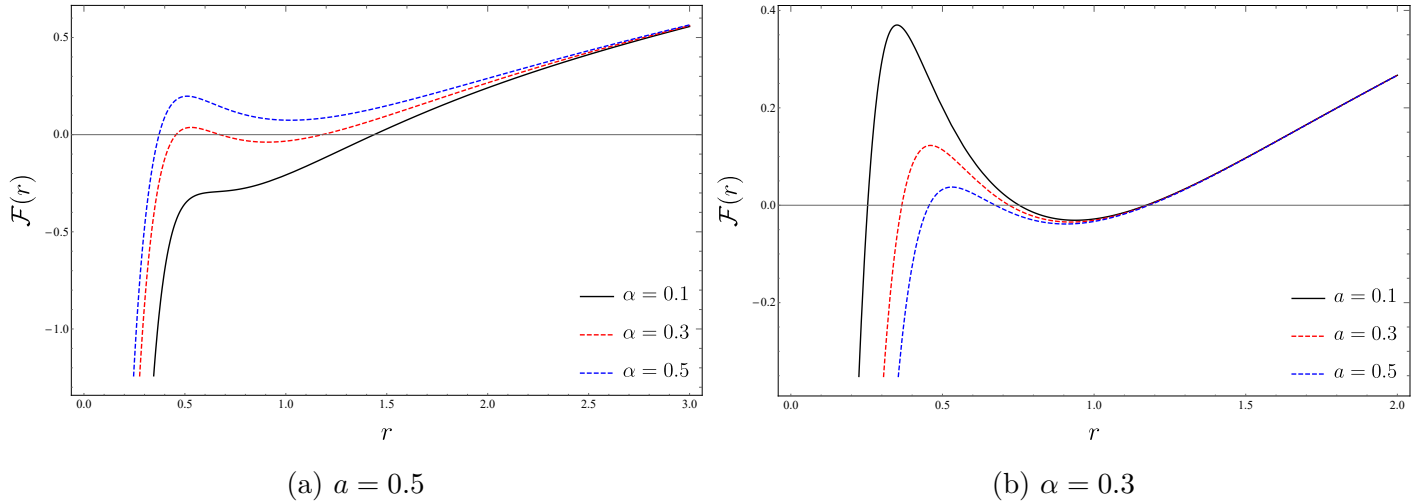


Figure 1: Plots of $\mathcal{F}(r)$ versus r for $M = 1$, $Q = 0.9$ and $\Lambda = -0.05$

3 Thermodynamics

In this section, we investigate the thermodynamic properties of EH AdS BH in 4D EGB gravity. The pioneering works of Bekenstein and Hawking [76, 77] established a fundamental connection between thermodynamic quantities and the geometric properties of BHs, identifying the entropy with the area of the event horizon and the temperature with the surface gravity. Consequently, all thermodynamic quantities of the BH are evaluated at the event horizon r_+ . In particular, the BH mass can be obtained from the horizon condition $\mathcal{F}(r_+) = 0$, yielding

$$M = \frac{r_+}{2} \left(1 + \frac{\alpha + Q^2}{r_+^2} - \frac{\Lambda r_+^2}{3} - \frac{aQ^4}{20r_+^6} \right). \quad (21)$$

Figure 2 displays the variation of the BH mass as a function of the event horizon radius r_+ . The mass exhibits a non-monotonic dependence on r_+ , characterized by the presence of a local maximum and a local minimum. These extrema correspond to turning points separating different BH branches. We find that increasing the GB coupling α enhances the maximum value of the mass and shifts its location toward smaller horizon radii, indicating that higher-curvature effects become dominant at shorter length scales. In contrast, increasing the EH parameter also increase the maximum mass but shift its location toward larger horizon radii. This behavior reflects the role of nonlinear field effects in delaying the onset of thermodynamic instability and extending the region of stability for small BHs. Consequently, the competing effects of higher-curvature gravity and nonlinear electrodynamics give rise to a rich phase structure and significantly modify the thermodynamic stability of the system.

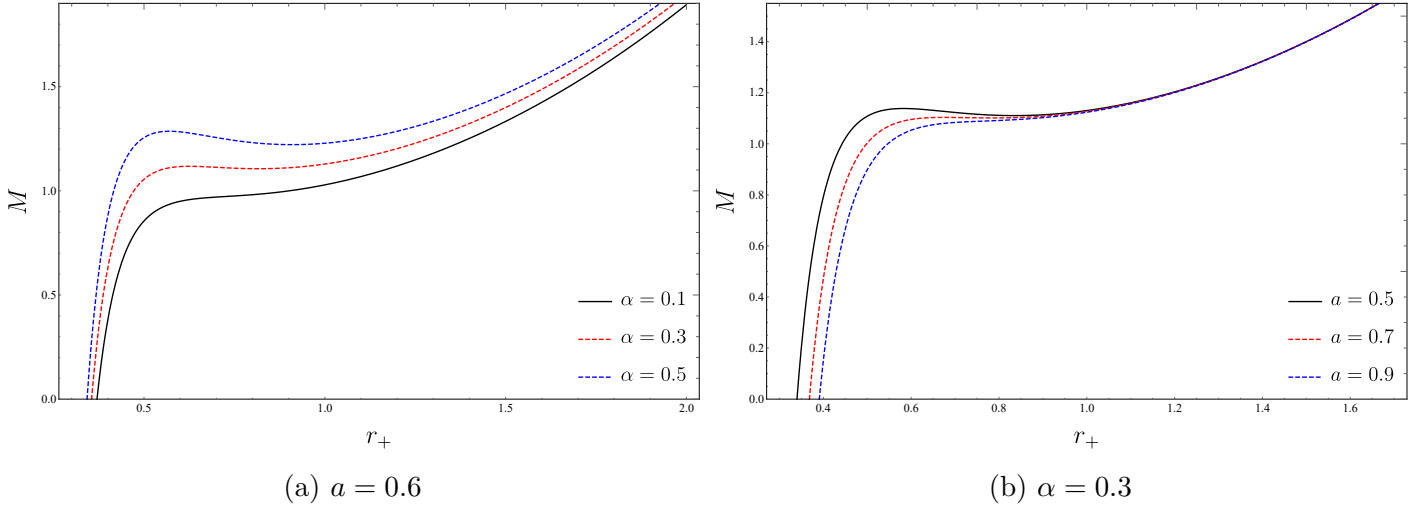


Figure 2: Plots of M versus r_+ for $Q = 0.9$ and $\Lambda = -0.5$

Further, we can define the Hawking temperature (T_H) in terms of the BH can be surface gravity (κ) as

$$T_H = \frac{\kappa}{2\pi} = \frac{1}{4\pi} \left. \frac{\partial \mathcal{F}(r)}{\partial r} \right|_{r=r_+} = \frac{1 - \frac{\alpha+Q^2}{r_+^2} - \Lambda r_+^2 + \frac{aQ^4}{4r_+^6}}{4\pi r_+ \left(1 + \frac{2\alpha}{r_+^2}\right)}. \quad (22)$$

Through the bounds of extended phase space, the negative value of Λ can be interpreted as a thermodynamic pressure P , defined as

$$P = -\frac{\Lambda}{8\pi}. \quad (23)$$

Substituting (23) into Eq. (22), the Hawking temperature can be rewritten as

$$T_H = \frac{1 - \frac{\alpha+Q^2}{r_+^2} + 8\pi P r_+^2 + \frac{aQ^4}{4r_+^6}}{4\pi r_+ \left(1 + \frac{2\alpha}{r_+^2}\right)}. \quad (24)$$

In the absence of EGB gravity ($\alpha = 0$), we can obtain

$$T_H = \frac{1}{4\pi r_+} \left(1 - \frac{Q^2}{r_+^2} + 8\pi P r_+^2 + \frac{aQ^4}{4r_+^6}\right), \quad (25)$$

which agrees with the result obtained in [78]. Furthermore, by setting $a = 0$, one recovers the standard Hawking temperature of the charged AdS BH

$$T_H = \frac{1}{4\pi r_+} \left(1 - \frac{Q^2}{r_+^2} + 8\pi P r_+^2\right). \quad (26)$$

Clearly, T_H of the EH AdS BH in 4D EGB gravity is modified by both the GB and EH parameters, indicating that the temperature is highly sensitive to higher-curvature and NLED effects (see Fig. 3). Figure 3 displays the Hawking temperature as a function of the horizon radius r_+ . The temperature exhibits a minimum, separating small and large BH phases. Decreasing the GB coupling α raises the temperature and shifts the minimum toward smaller horizon radii, indicating the dominance of higher-curvature effects at short length scales. In contrast, increasing the EH parameter shifts the minimum toward larger r_+ reflecting the influence of NLED. These results show that higher-curvature and NLED corrections affect the thermal behavior in competing ways.

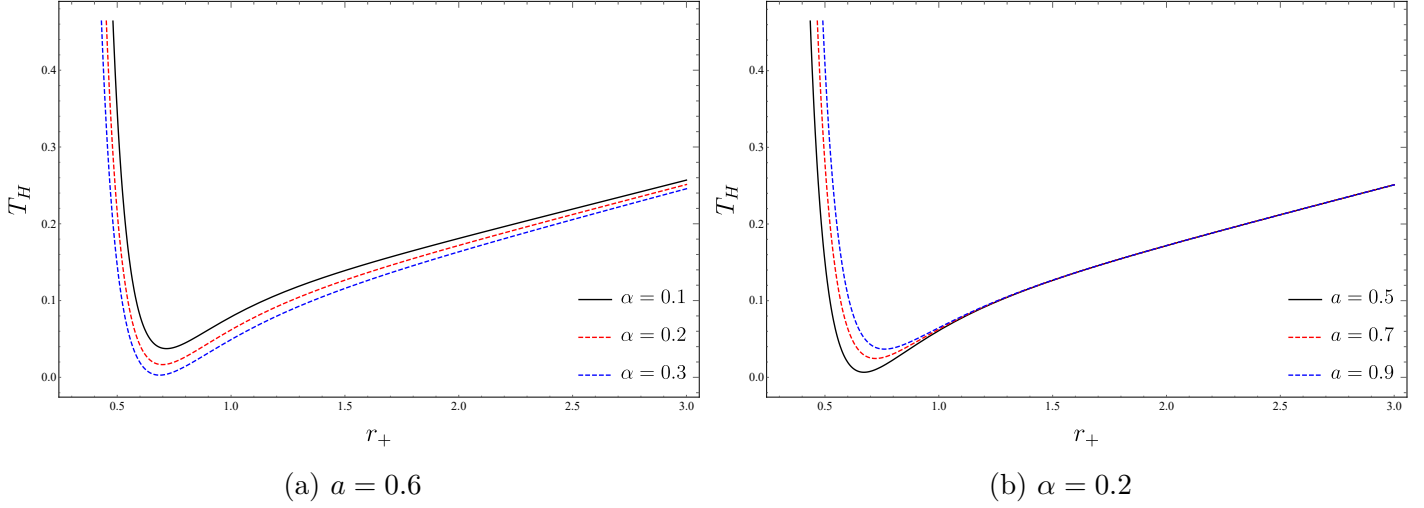


Figure 3: Plots of T_H versus r_+ for $Q = 0.9$ and $P = \frac{1}{8\pi}$

In the framework of extended phase space, the generalized first law of BH for the considered BH can be expressed as

$$dM = TdS + \Phi dQ + VdP. \quad (27)$$

Using the first law in Eq. (27), the Bekenstein entropy is obtained as

$$S = \int \frac{dM}{T} = \int 2\pi r_+ \left(1 + \frac{2\alpha}{r_+^2}\right) dr_+ = \pi r_+^2 + 4\alpha \ln r_+. \quad (28)$$

The logarithmic correction encodes the contribution of higher-order curvature terms associated with the GB invariant, resulting in a modification of the standard area law. Another notable example of a quantity in thermodynamics is the specific heat capacity at constant pressure C_P , which describes the local thermodynamic stability of the BH. In the present case, it is given by

$$C_P = \left(\frac{dM}{dT}\right)_P = -\frac{2\pi r_+^2 \left(1 + \frac{2\alpha}{r_+^2}\right)^2 \left(1 + \frac{aQ^4}{4r_+^6} - \frac{Q^2 + \alpha}{r_+^2} + 8\pi P r_+^2\right)}{\left(1 - 3\frac{\alpha + Q^2}{r_+^2} - 8\pi P r_+^2 + \frac{7aQ^4}{4r_+^6}\right) - \frac{2\alpha}{r_+^2} \left(1 + \frac{Q^2 + \alpha}{r_+^2} + 24\pi P r_+^2 - \frac{5aQ^4}{4r_+^6}\right)}. \quad (29)$$

The local thermodynamic stability is governed by the sign of the heat capacity, whose divergence occurs when $\frac{dT}{dr_+} = 0$ corresponding to the minimum of the Hawking temperature at $r_+ = r_{\min}$. For $r_+ < r_{\min}$ the heat capacity is negative (Fig.4), indicating thermodynamic instability, while for $r_+ > r_{\min}$ it becomes positive, signaling a stable large BH phase; this divergence therefore marks a second-order phase transition. Increasing the GB coupling shifts the divergence point toward smaller horizon radii, reflecting the dominance of higher-curvature effects at short length scales. In contrast, increasing the EH parameter moves the divergence toward larger r_+ , demonstrating the competing influence of NLED on the thermodynamic phase structure.

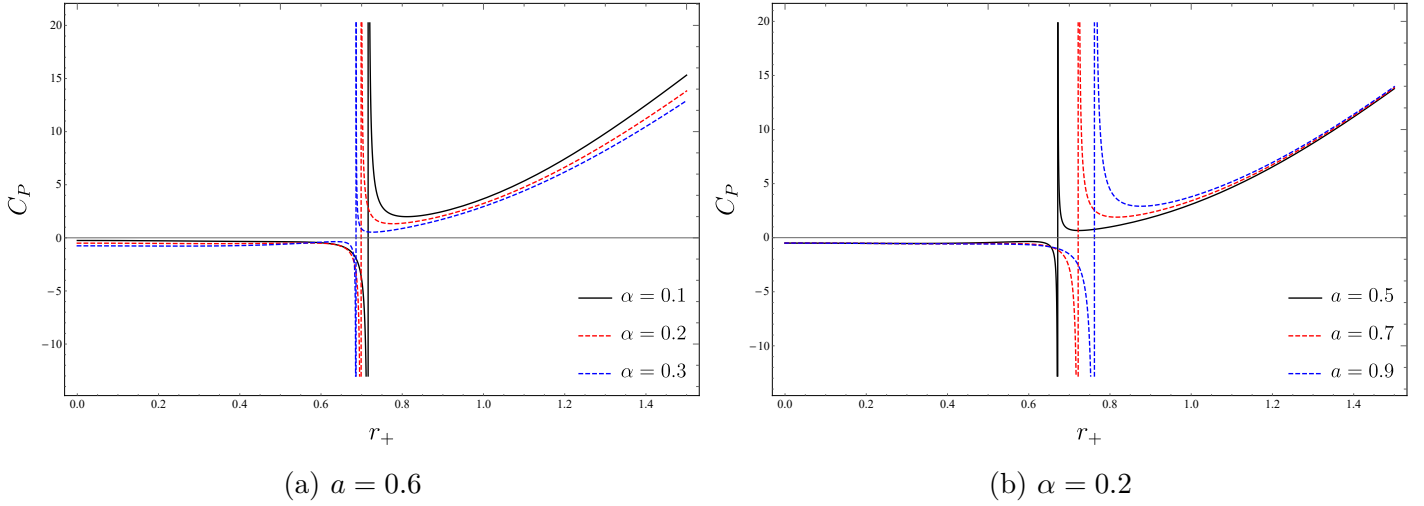


Figure 4: Plots of C_P versus r_+ for $Q = 0.9$ and $P = \frac{1}{8\pi}$

Now, using Eq. (24), we derive the equation of state, which after rearrangement takes the form

$$P = \frac{1}{2r_+} \left(1 + \frac{2\alpha}{r_+^2} \right) T_H + \frac{\alpha + Q^2}{8\pi r_+^4} - \frac{aQ^4}{32\pi r_+^8} - \frac{1}{8\pi r_+^2}. \quad (30)$$

Therefore, Eq.(30) can be regarded as $P = P(r_+, T)$, representing the equation of state in the extended phase space. This expression is usually referred to as the geometric equation of state. Fig.5 displays the pressure isotherms in the extended phase space, revealing a non-monotonic behavior characteristic of critical phenomena. The maximum of each isotherm corresponds to the critical point separating distinct thermodynamic phases. Increasing the GB coupling raises the peak pressure, indicating that higher-curvature effects enhance the effective repulsive interactions and shift the critical point to higher pressures. In contrast, increasing the EulerHeisenberg parameter lowers the maximum pressure, reflecting the screening effect of NLED and shifting the critical point toward lower pressures.

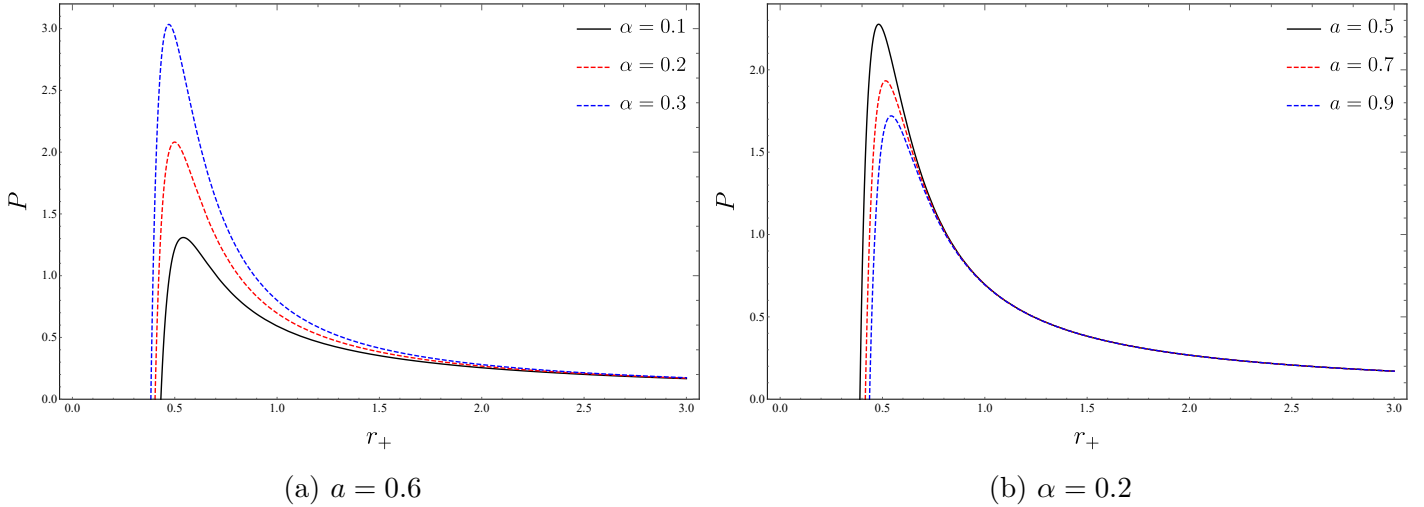


Figure 5: Pressure P versus horizon radius r_+ for $Q = 0.9$ and $P = \frac{1}{8\pi}$

The critical parameters can be obtained by requiring

$$\left. \frac{\partial}{\partial r} P \right|_{r=r_c} = 0, \quad \left. \frac{\partial^2}{\partial r^2} P \right|_{r=r_c} = 0. \quad (31)$$

For these conditions, we can obtain the critical values as

$$T_c = \frac{1 + \frac{aQ^4}{r_c^6} - 2\frac{Q^2+\alpha}{r_c^2}}{2\pi r_c \left(1 + \frac{6\alpha}{r_c^2}\right)}, \quad (32)$$

$$P_c = -\frac{aQ^4}{32\pi r_c^8} + \frac{\left(1 + \frac{2\alpha}{r_c^2}\right) \left(1 + \frac{aQ^4}{r_c^6} - 2\frac{Q^2+\alpha}{r_c^2}\right)}{4\pi r_c^2 \left(1 + \frac{6\alpha}{r_c^2}\right)} + \frac{\alpha + Q^2}{8\pi r_c^4} - \frac{1}{8\pi r_c^2}. \quad (33)$$

Here r_c is the solution of the following algebraic equation:

$$12\alpha^2 r_c^4 + 6Q^2 r_c^6 \left(1 + \frac{2\alpha}{r_c^2}\right) - r_c^8 + 12\alpha r_c^6 - aQ^4 (30\alpha + 7r_c^2) = 0. \quad (34)$$

Since an analytic solution of this equation is not tractable, we solve it numerically. The resulting critical parameters for varying α and EH couplings are summarized in Table 1. As shown in the table, increasing α , leads to a monotonic increase in the critical radius r_c , while both T_c and P_c decrease. This behavior indicates that the GB term significantly affects the location of the critical point. In contrast, varying the EH parameter a produces only small changes in the critical quantities. In particular, r_c decreases slightly, whereas T_c and P_c increase marginally as a increases, suggesting that the influence of the EH correction on the critical behavior is comparatively weak.

$a = 0.4$				$\alpha = 0.3$			
α	r_c	T_c	P_c	a	r_c	T_c	P_c
0.1	2.27274	4.4838×10^{-2}	2.80444×10^{-3}	0.1	2.80444	3.51464×10^{-2}	2.28976×10^{-3}
0.3	2.80169	3.51581×10^{-2}	2.29168×10^{-3}	0.3	2.80261	3.51542×10^{-2}	2.29104×10^{-3}
0.5	3.2373	2.99118×10^{-2}	1.67694×10^{-3}	0.5	2.80076	3.5162×10^{-2}	2.29233×10^{-3}
0.7	3.61823	2.64878×10^{-2}	1.32353×10^{-3}	0.7	2.79891	3.51699×10^{-2}	2.29362×10^{-3}
0.9	3.96156	2.40254×10^{-2}	1.09356×10^{-3}	0.9	2.79704	3.51778×10^{-2}	2.29493×10^{-3}

Table 1: Critical quantities r_c , T_c and P_c for varying α and the EH parameter.

4 Joule Thomson Expansion

In this section, we analyze the Joule Thomson (JT) expansion in the scenario of considered BH. The JT mechanism constitutes a key thermodynamic pathway in which enthalpy remains invariant while temperature adjusts according to pressure variations. Within the BH formalism, it corresponds to an isenthalpic transformation in the extended phase space. The governing measure is the JT coefficient μ_J , which relates pressure changes with temperature evolution and denotes whether the BH undergoes thermal contraction or expansion. Making use of the definitions of thermodynamic pressure, entropy and temperature, the BH EoS can be written as

$$\mu_J = \left(\frac{\partial T}{\partial P}\right)_H, \quad (35)$$

where H denotes the enthalpy. When the expansion causes a decrease in pressure, the temperature may either rise or drop, with the sign of μ specifying the outcome: $\mu < 0$ corresponds to heating, while $\mu > 0$ signals cooling. Following the formulation, the JT coefficient can be recast in the alternative form

$$\mu_J = \left(\frac{\partial T}{\partial P}\right)_M = \frac{1}{C_P} \left[T \left(\frac{\partial V}{\partial T}\right)_P - V \right], \quad (36)$$

where C_P is the specific heat at constant pressure. Also, the condition for obtaining the inversion temperature arises from setting $\mu = 0$, yielding

$$T_i = V \left(\frac{\partial T}{\partial V} \right)_P. \quad (37)$$

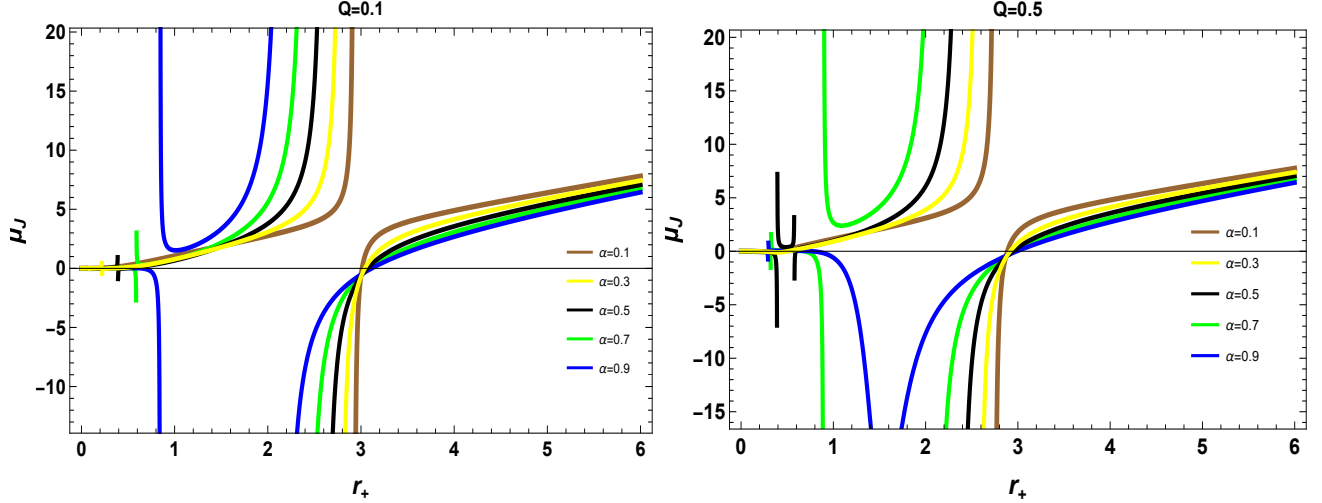


Figure 6: Plots of μ_J versus r_+ with $a = 0.9$, $M = 1$.

In this section, we investigate the JT expansion of the considered BH within the extended phase space framework that incorporates NLED effects. In such a thermodynamic setting, the variation of temperature with respect to pressure defines the expansion process, whereas the enthalpy remains unchanged. Since in AdS backgrounds the BH mass is interpreted as enthalpy, it consequently remains fixed during the expansion process. A straightforward approach to evaluate the JT coefficient μ can be achieved by carefully analyzing the relations among the thermodynamic quantities. In this case, the pressure can be recast in terms of the event horizon radius, the coupling constant and the mass of the BH, illustrated as

$$P(M, r_+) = \frac{60r_+^4 (\alpha - 2Mr_+ + Q^2 + r_+^2) - 3aQ^4}{160\pi r_+^8}, \quad (38)$$

and substituting this form of $P(M, r_+)$ into the temperature relation (24), the expression for the Hawking temperature becomes

$$T(M, r_+) = \frac{aQ^4 - 5r_+^4 (2\alpha - 3Mr_+ + 2Q^2 + r_+^2)}{10r_+^5 (2\alpha + \pi r_+^2)}. \quad (39)$$

By employing the relations that connect the pressure and temperature, one can evaluate the JT coefficient μ_J , which is defined as

$$\mu_J = \left(\frac{\partial T}{\partial P} \right)_M = \left(\frac{\partial T}{\partial r_+} \right)_M \left(\frac{\partial r_+}{\partial P} \right)_M = \frac{(\partial T / \partial r_+)_{M}}{(\partial P / \partial r_+)_{M}}. \quad (40)$$

This expression reduces to

$$\mu_J = \frac{4\pi r_+^3 (aQ^4 (8\alpha + 5\pi r_+^2) - 4r_+^4 (4\alpha^2 + \pi r_+^2 (8\pi P r_+^4 + 3Q^2 - 2r_+^2) + 4\alpha Q^2 + (3\pi - 2)\alpha r_+^2))}{3(2\alpha + \pi r_+^2)^2 (4r_+^4 (\alpha + 8\pi P r_+^4 + Q^2 - r_+^2) - aQ^4)}. \quad (41)$$

Figure (6) illustrates how the JT coefficient, μ_J , changes depending on the event horizon radius r_+ for various values of GB parameter α and electric charge Q . It can be noted that the greater the α , the more the inversion points move towards greater horizon radii which means the corrections with respect to the higher curvature are more dominant on the expansion factor. The charge Q also greatly influences the μ_J values, which supports more of the electro-magnetic component of the response to the changes in the thermodynamic system. The change of sign in μ_J distinguishes the cooling and heating sections and it indicates that the JT expansion is not trivial. This illustrates the combined influences of curvature and charge on the thermodynamic properties of BHs.

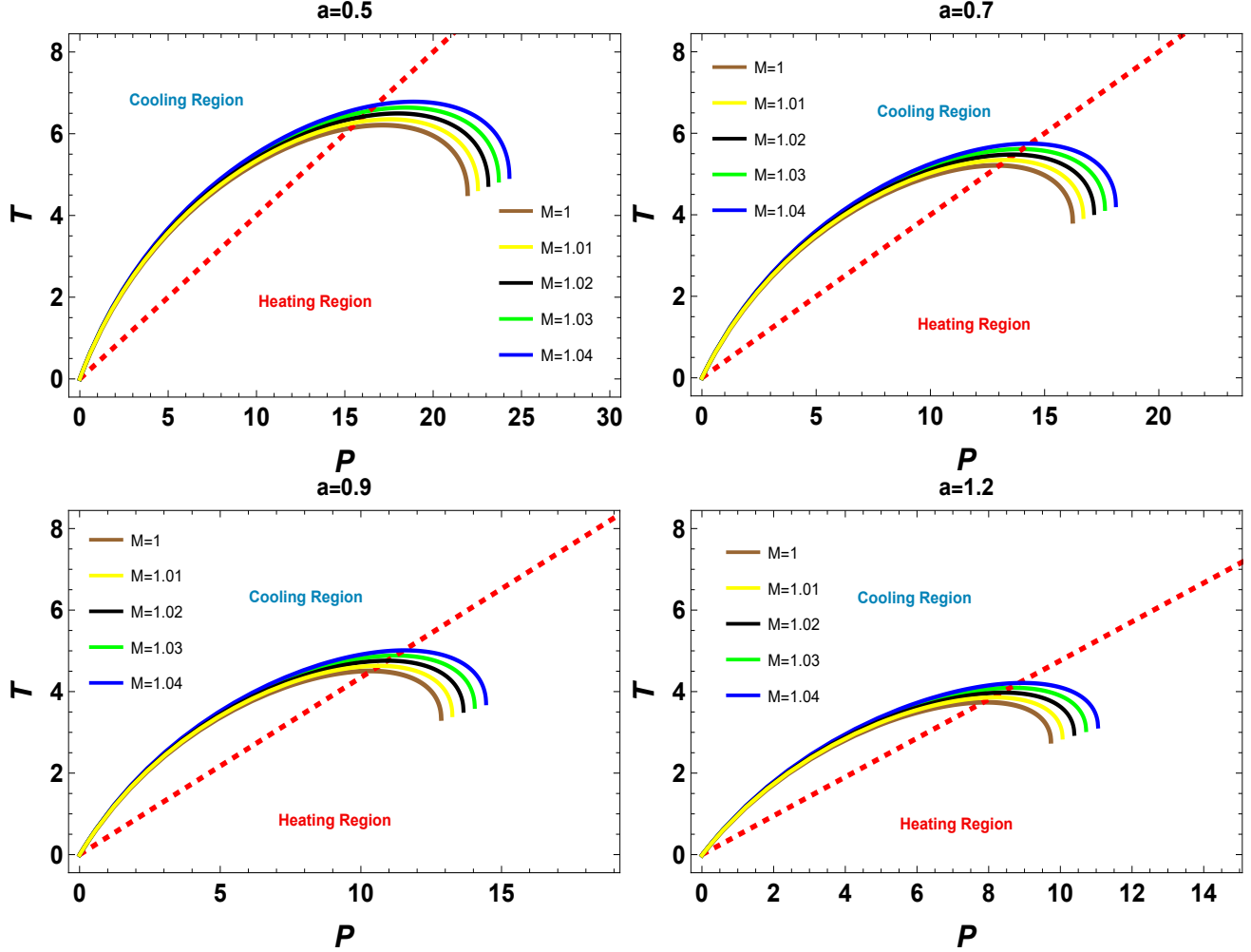


Figure 7: Isenthalpic and inversion plots in $T - P$ plane for distinct choices of a with $Q = 0.65, \alpha = 0.2$.

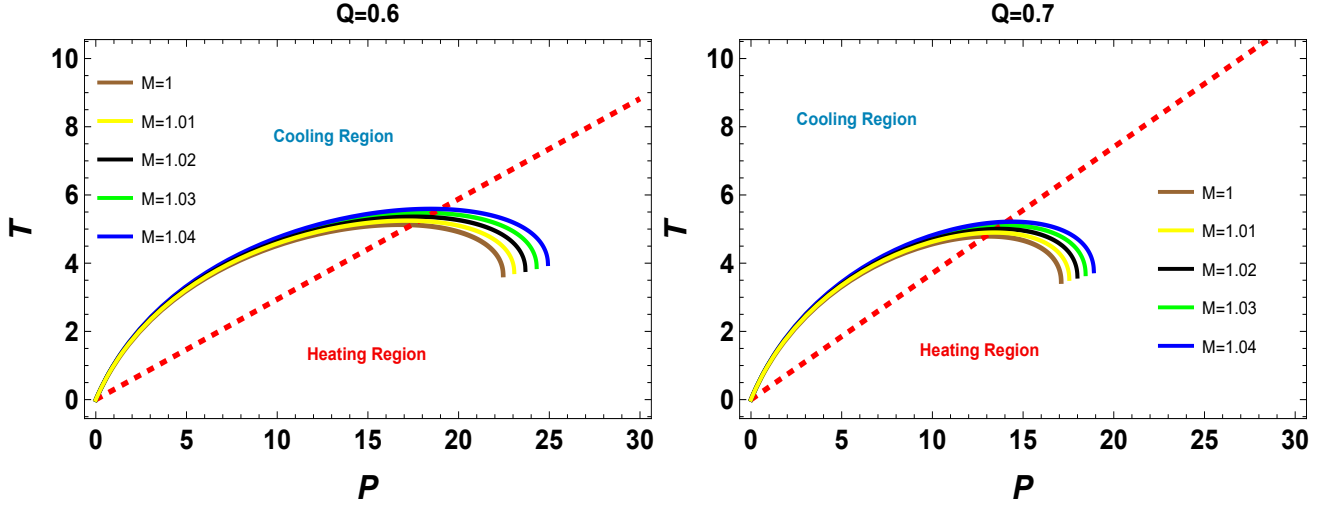


Figure 8: Isenthalpic and inversion plots in $T - P$ plane for distinct choices of Q with $a = 0.6, \alpha = 0.3$.

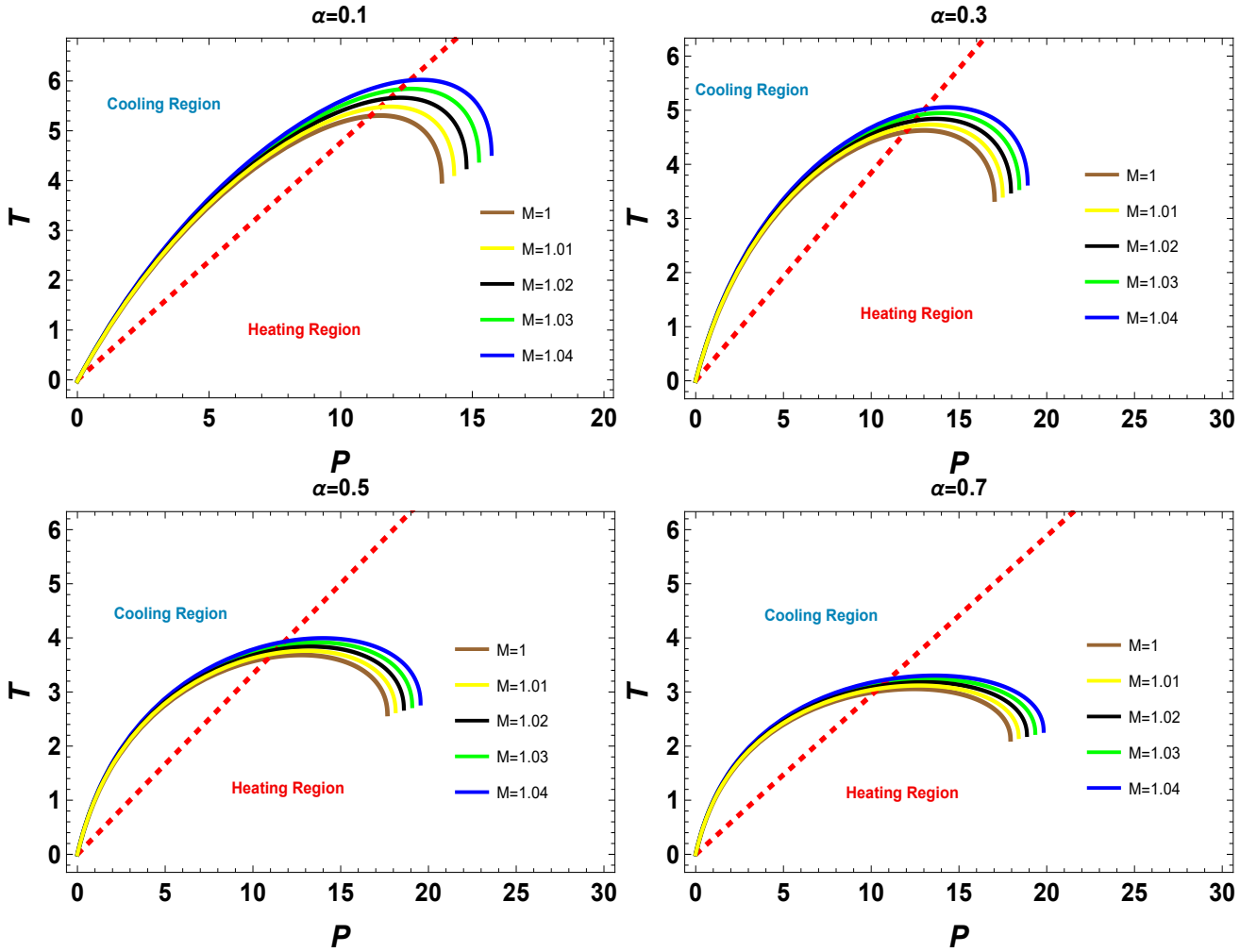


Figure 9: Isenthalpic and inversion plots in $T - P$ plane for distinct choices of α with $Q = 0.65, a = 0.7$.

Starting with the condition $\mu_J = 0$ in Eq.(41), one arrives at the following relation:

$$4\pi r_{ci}^3 (aQ^4 (8\alpha + 5\pi r^2) - 4r_{ci}^4 (4\alpha^2 + 4\alpha Q^2 + \pi r_{ci}^2 (3Q^2 - 2r_{ci}^2) + (3\pi - 2)\alpha r_{ci}^2)) = 0. \quad (42)$$

Under this framework, the parameter P_i is interpreted as the inversion pressure. The valid solution of Eq. (42), i.e., the positive real root, determines the associated horizon radius r_{ci} .

Furthermore, the explicit formula for the inversion temperature takes the form

$$T_i = -\frac{(aQ^4(10\alpha + 7\pi r_{ci}^2) + 4r_{ci}^4(\pi r_{ci}^2(-3\alpha + 48\alpha P_i r_{ci}^2 - 3Q^2 + r_{ci}^2) + 8\pi^2 P_i r_{ci}^6 - 2\alpha(\alpha + Q^2 + r_{ci}^2)))}{48r_{ci}^5(2\alpha + \pi r_{ci}^2)^3(\pi r_{ci}^2 + 4\alpha \log(r_{ci}))^{-1}} \quad (43)$$

Further, we can find

$$\begin{aligned} T_i &= -\frac{(\pi r_{ci}^2 + 4\alpha \log(r_{ci}))(aQ^4 + r_{ci}^4(-2\alpha - 2Q^2 + r_{ci}^2))}{4r_{ci}^5(6\alpha^2 + \pi^2 r_{ci}^4 + 3\pi\alpha r_{ci}^2 - 2\alpha(6\alpha + \pi r_{ci}^2)\log(r))}, \\ P_i &= (aQ^4(\alpha + \pi r_{ci}^2)(6\alpha + 5\pi r_{ci}^2) + 2\alpha \log(r_{ci})(aQ^4(10\alpha + 7\pi r_{ci}^2) + 4\pi r_{ci}^6(-3\alpha - 3Q^2 + r_{ci}^2) \\ &\quad - 8\alpha r_{ci}^4(\alpha + Q^2 + r_{ci}^2)) - 4r_{ci}^4(6\alpha^2(\alpha + Q^2 - r_{ci}^2) + \pi\alpha r_{ci}^2(7\alpha + 7Q^2 - 5r_{ci}^2) + \pi^2 r_{ci}^4(3\alpha + 3Q^2 - 2r_{ci}^2))) \\ &\quad \times (32\pi r_{ci}^8(6\alpha^2 + \pi^2 r_{ci}^4 + 3\pi\alpha r_{ci}^2 - 2\alpha(6\alpha + \pi r_{ci}^2)\log(r_{ci})))^{-1} \end{aligned}$$

If one considers the special case $P_i = 0$ in Eq. (43), this reduces to the lowest attainable inversion temperature, given by

$$T_i^{min} = -\frac{(\pi r_{ci}^2 + 4\alpha \log(r_{ci}))(aQ^4(10\alpha + 7\pi r_{ci}^2) + 4\pi r_{ci}^6(-3\alpha - 3Q^2 + r_{ci}^2) - 8\alpha r_{ci}^4(\alpha + Q^2 + r_{ci}^2))}{48r_{ci}^5(2\alpha + \pi r_{ci}^2)^3}.$$

In Figures (7)-(9), we see the isenthalpic curves and inversion trajectories for the JouleThomson expansion of the charged EulerHeisenbergAdS BH in 4D EGB gravity in the TP Plane. In all the figures, the inversion curve separates the thermodynamic phase space into the cooling ($\mu_J > 0$) and heating ($\mu_J < 0$) regions. This reinforces the idea of the JouleThompson expansion being nontrivial and similar to real fluids. The isenthalpic curves for different masses of the BH do intersect the inversion curve at different points. Beyond these points the nature of the thermodynamic response shifts. In Figure (7), we see how the parameter of the EulerHeisenberg a affects JouleThomson expansion. When a increases, the JouleThomson inversion curve shifts to lower pressures and lower temperatures. This means strong nonlinear electromagnetic corrections limit the cooling region. Additionally, for larger a , the inversion curve becomes steeper. This reflects that the sensitivity of BH temperature to changes in pressure increases. This shows how important NLED is in changing the thermodynamic phase structure of BHs. Figure (8) analyze the effects that the electric charge Q has while the GB coupling and the nonlinear parameter are held constant. An increase in Q raises both the inversion temperature and inversion pressure. This also increases the size of the cooling region in the $T - P$ plane. This is due to the increase in electromagnetic repulsion, which increases the thermal response of the BH when the expansion is isenthalpic. Therefore, the charged BHs will display more significant JT cooling effects than the weakly charged configurations. Figure (9) shows how the JT expansion changes with the Gauss-Bonnet coupling α . It appears that with the increase of α the inversion curve moves to higher pressures and the inversion temperature slightly decreases, which shows that the corrections of high curvature are important to the expansion dynamics. The adjustments of α comments on the effective equation of state which in turn changes the interplay of gravitational pull and thermodynamic pressure. It shows that the GB corrections are vital in the modifications of the heating and cooling transition of the BH system.

5 Geodesic Equations

In gravitational theories, geodesic motion provides a direct link between the geometry of spacetime and the dynamics of free test particles. The trajectories of these particles encode information about

the curvature and symmetries of the underlying metric. In the framework of EGB gravity coupled to EH NLED, this analysis becomes particularly relevant, since the presence of additional fields modifies the spacetime geometry. Consequently, the study of test particle motion offers an effective approach to examine deviations from the predictions of general relativity induced by EGB gravity and NLED. The investigation of geodesic motion is not limited to describing particle trajectories; it also provides insight into observable effects such as light deflection, orbital dynamics, and photon propagation. Examining these trajectories enables one to understand the BH structure and the effects of a vector field on gravity. Now, we consider the Lagrangian to analyze the geodesic of considered BH given in Eq. (18) as

$$L = \frac{1}{2} g_{\mu\nu} \dot{x}^\mu \dot{x}^\nu, \quad (44)$$

where $\dot{x} = dx/d\tau$. The metric from Eq. (18) allows the Lagrangian to be expressed as

$$\mathcal{L} = \frac{1}{2} \left[r^2 \left(\frac{d\theta}{d\tau} \right)^2 - \mathcal{F}(r) \left(\frac{dt}{d\tau} \right)^2 + \frac{1}{\mathcal{F}(r)} \left(\frac{dr}{d\tau} \right)^2 + r^2 \sin^2 \theta \left(\frac{d\varphi}{d\tau} \right)^2 \right]. \quad (45)$$

The Euler-Lagrange equations provide the principles of motion

$$\frac{d}{d\tau} \left(\frac{\partial}{\partial \dot{x}^\sigma} \mathcal{L} \right) - \left(\frac{\partial}{\partial x^\sigma} \mathcal{L} \right) = 0. \quad (46)$$

Conservation of energy E and angular momentum L arise as conserved quantities because the metric does not depend on the coordinates t and φ respectively. Mathematically, we can define

$$E = \mathcal{F}(r) \left(\frac{dt}{d\tau} \right), \quad (47)$$

$$L = r^2 \sin^2 \theta \left(\frac{d\varphi}{d\tau} \right). \quad (48)$$

These quantities correspond to conserved parameters associated with timelike and axial Killing vectors and are measured by static observers at spatial infinity. The equation governing the polar motion is obtained as

$$r^2 \left(\frac{d^2\theta}{d\tau^2} \right) + 2r \left(\frac{dr}{d\tau} \right) \left(\frac{d\theta}{d\tau} \right) - r^2 \sin \theta \cos \theta \left(\frac{d\varphi}{d\tau} \right)^2 = 0. \quad (49)$$

Fixing the Lagrangian as $\mathcal{L} = -\frac{\epsilon}{2}$, where for massive particles ($\epsilon = 1$) and null geodesics ($\epsilon = 0$), we obtain

$$\mathcal{F}(r) \left(\frac{dt}{d\tau} \right)^2 - \frac{1}{\mathcal{F}(r)} \left(\frac{dr}{d\tau} \right)^2 - r^2 \left(\frac{d\theta}{d\tau} \right)^2 - r^2 \sin^2 \theta \left(\frac{d\varphi}{d\tau} \right)^2 = \epsilon. \quad (50)$$

Using the conserved quantities, we get

$$\left(\frac{dr}{d\tau} \right)^2 = E^2 - \mathcal{F}(r) \left(\epsilon + \frac{L^2}{r^2 \sin^2 \theta} \right). \quad (51)$$

Alternatively, this equation takes the form

$$\dot{r}^2 = E^2 - V_{\text{eff}}(r), \quad (52)$$

we obtain

$$V_{\text{eff}}(r) = \mathcal{F}(r) \left(\epsilon + \frac{L^2}{r^2 \sin^2 \theta} \right). \quad (53)$$

Eq. (47), Eq. (48), Eq. (52) and Eq. (53) provide the basis for the analysis of geodesic motion in the considered spacetime.

5.1 Orbital geodesics of massive particles

Here, we investigate the geodesic motion of massive particles with nonvanishing angular momentum $L \neq 0$ in the equatorial plane ($\theta = \frac{\pi}{2}$). For timelike geodesics ($\epsilon = 1$), the effective potential takes the form

$$V_{\text{eff}}(r) = \left(1 + \frac{r^2}{2\alpha} \left(1 - \sqrt{1 + \frac{4\alpha}{r^2} \left(\frac{2M}{r} - \frac{Q^2}{r^2} + \frac{\Lambda}{3}r^2 + \frac{aQ^4}{20r^6} \right)} \right) \right) \left(1 + \frac{L^2}{r^2} \right). \quad (54)$$

By varying α and a , we observe the behavior of $V_{\text{eff}}(r)$ shown in Figure 10. The detailed explanation is presented as:

- Panel (10a) of Fig.10 shows the effective potential for various values of the Gauss–Bonnet coupling parameter. As α increases, the height of the potential barrier increases and its maximum shifts slightly away from the event horizon. This effect becomes less pronounced at larger radial distances.
- Panel (10b) displays the influence of the EH NLED parameter. Increasing a leads to a decrease in the maximum of the effective potential, while the location of the peak moves outward, indicating a modification of the orbital structure induced by NLED effects.

The effective potential determines the orbital properties of massive particles in the considered spacetime. In general, the existence of local minima in $V_{\text{eff}}(r)$ corresponds to stable circular orbits, while local maxima are associated with unstable circular trajectories. The height and location of these extrema therefore play a crucial role in determining the stability and admissible regions of particle motion. The dependence of the effective potential on the GB coupling parameter α , indicates that higher-curvature corrections significantly influence the orbital dynamics near the BH. As α increases, the enhancement of the potential barrier suggests that massive particles require higher energy to access regions close to the event horizon. However, the decreasing influence of α at larger radial distances implies that GB effects are primarily relevant in the strong-field regime, while the spacetime gradually approaches the general relativistic behavior far from the BH. The contribution of the EH NLED parameter a leads to a noticeable modification of the effective potential. The reduction in the height of the potential maximum with increasing a indicates a weakening of the repulsive contribution associated with nonlinear electromagnetic effects. This behavior suggests that NLED may facilitate the inward motion of massive particles and alter the conditions for stable circular orbits when compared to the linear Maxwell case. Overall, these results demonstrate that both higher-curvature corrections and nonlinear electrodynamic effects introduce nontrivial modifications to the geodesic structure of the spacetime. The combined influence of these parameters leads to significant deviations from the standard scenarios, particularly in the vicinity of the BH, thereby affecting the existence and stability of massive particle orbits.

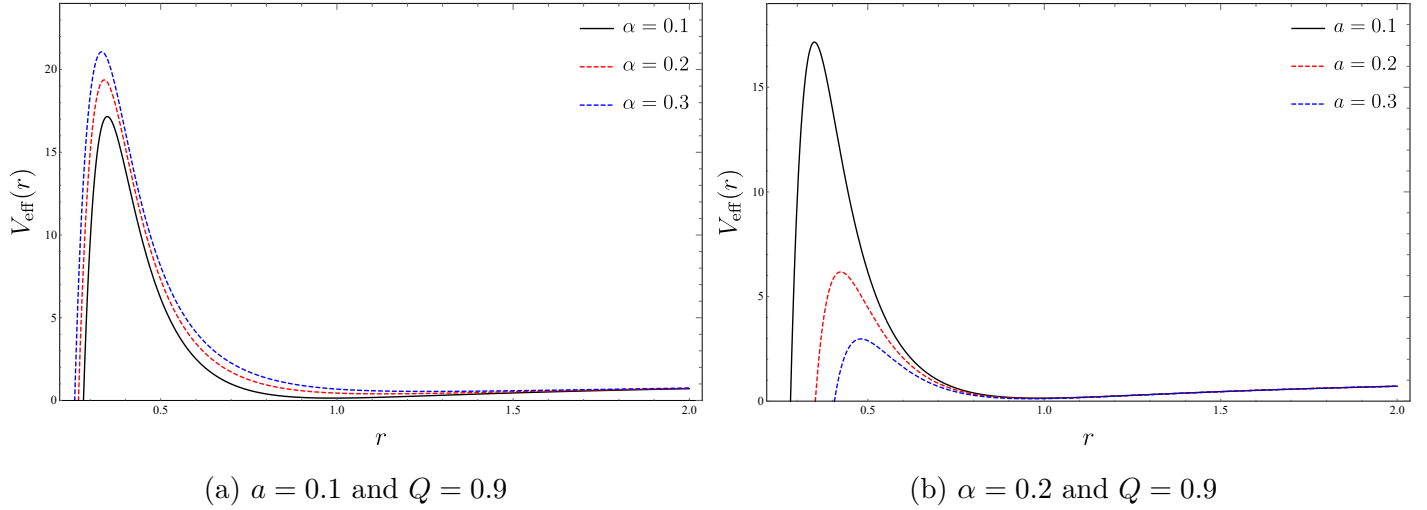


Figure 10: Effective potential V_{eff} for massive test particles versus r for $M = 1$ and $\Lambda = -0.1$.

We now examine the motion of test particles along nonradial timelike geodesics by focusing on their orbital dynamics. The nature of the resulting trajectories is determined by the value of the conserved energy E , allowing the motion to be classified into several distinct regimes:

$E > E_{\text{uns}}$: The absence of radial turning points implies that particles are inevitably captured by the BH. In this regime, the gravitational attraction dominates over the centrifugal barrier, resulting in plunge-type trajectories. Such orbits are characteristic of the strong-field region and are particularly sensitive to higher-curvature and nonlinear electrodynamic corrections.

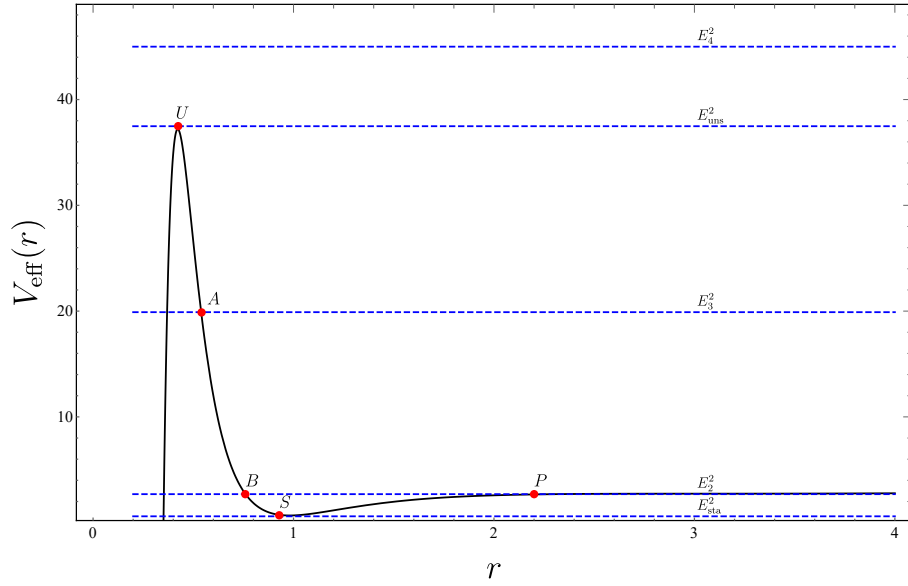
$E = E_{\text{uns}}$: The particle occupies an unstable circular orbit located at the maximum of the effective potential. This configuration represents the threshold between plunging and escaping trajectories. Any small perturbation causes the particle either to fall into the BH or to move away toward large radial distances, reflecting the marginal stability of this orbit.

$E = E_3$: Particles approach the BH from large distances, reach a minimum radial position, and are subsequently deflected back. This regime corresponds to scattering-type trajectories and is directly related to gravitational deflection phenomena in the considered spacetime.

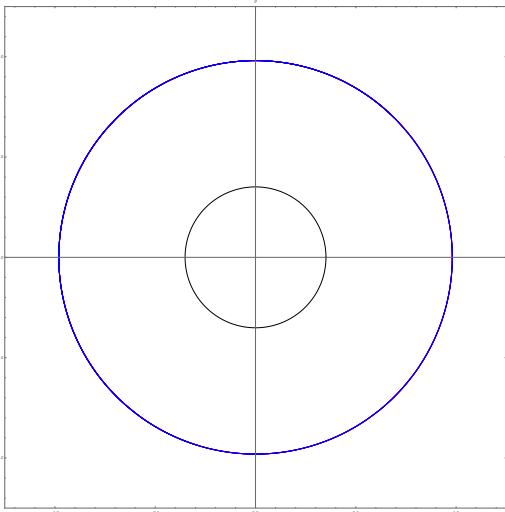
$E = E_2$: The effective potential exhibits two turning points, allowing for bound motion. In this case, particles oscillate between perihelion and aphelion distances, forming stable bound orbits governed by a balance between gravitational attraction and centrifugal effects.

$E = E_{\text{sta}}$: The particle follows a stable circular orbit located at the minimum of the effective potential. Small radial perturbations about this radius lead to bounded oscillations, indicating local stability.

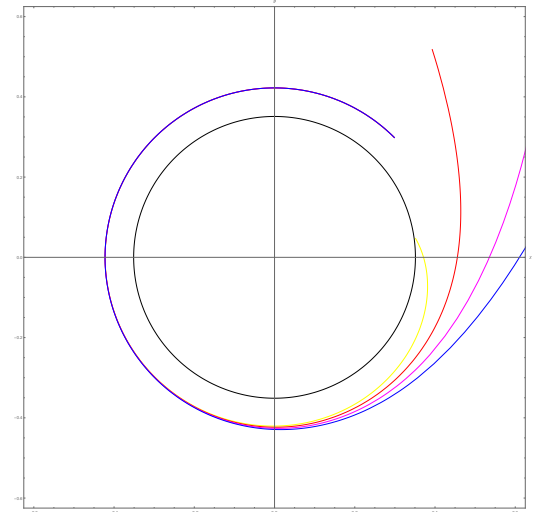
These results show that the energy dependent structure of timelike geodesics is significantly modified by GB and EH corrections in the strong-field regime, while the standard behavior is recovered at larger radial distances.



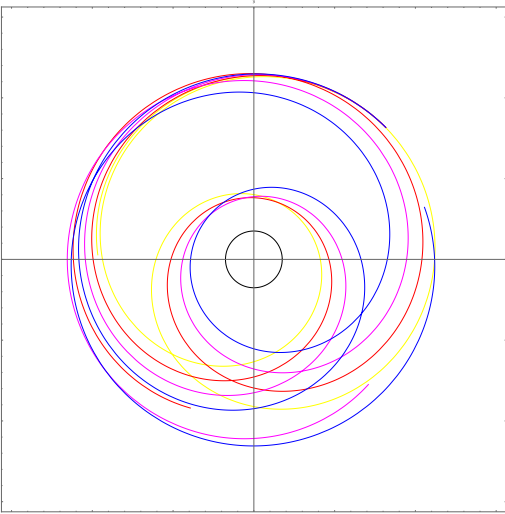
(a) Effective potential



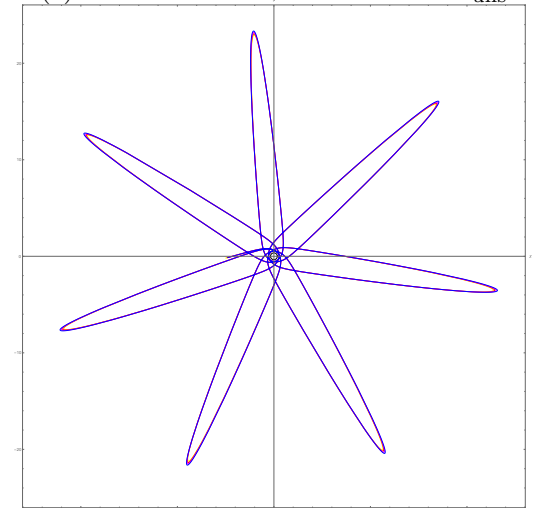
(b) stable circular orbit: $E = E_{sta}$



(c) unstable circular orbit: $E = E_{uns}$



(d) plunging trajectory: $E = E_2$



(e) bound orbit with two turning points: $E = E_3$

Figure 11: Effective potential and possible timelike particle motions in the 4D EGBEulerHeisenberg BH spacetime. Parameters: $M = 1$, $Q = 0.9$, $a = 0.2$, $\alpha = 0.2$, $\Lambda = -0.1$ and $L = 4$.

In the following, we investigate circular trajectories and their stability in order to assess how the deformed spacetime geometry affects this class of motion. Circular orbits are characterized by the simultaneous conditions that the radial velocity and radial acceleration vanish, namely

$$\dot{r} = \ddot{r} = 0, \quad (55)$$

and the corresponding effective potential must satisfy

$$V_{\text{eff}}(r) = E^2, \quad \frac{d}{dr}V_{\text{eff}}(r) = 0. \quad (56)$$

The stability of circular geodesics is determined by the effective potential behavior in the vicinity of the circular orbit radius. A circular orbit is stable if the effective potential attains a local minimum, which requires

$$\left. \frac{d^2}{dr^2}V_{\text{eff}}(r) \right|_{r=r_{\text{sta}}} > 0, \quad (57)$$

whereas a local maximum,

$$\left. \frac{d^2}{dr^2}V_{\text{eff}}(r) \right|_{r=r_{\text{uns}}} < 0. \quad (58)$$

Numerical solutions of Eq. (56) are presented in Table 2, where the radii of stable and unstable circular orbits are listed for various values of the GB coupling α and the EH parameter a . The table illustrates how the locations of both stable and unstable circular orbits depend on the α and a . The numerical results indicate that the GB coupling has a significant impact on orbital stability. As α increases, the radius of the stable circular orbit shifts toward larger values, while the corresponding unstable orbit moves inward. This trend suggests that higher-curvature corrections tend to enhance the range of stable circular motion for massive particles. By contrast, variations in the EH parameter produce an opposite effect. Increasing a results in a reduction of the radius of stable circular orbits, accompanied by an outward displacement of unstable circular orbits. This behavior reflects the role of NLED effects in altering the interplay between gravitational attraction and centrifugal forces, thereby narrowing the region of stable circular motion.

$a = 0.1$			$\alpha = 0.2$		
α	r_{sta}	r_{uns}	a	r_{sta}	r_{uns}
0.1	0.81657	0.360482	0.1	0.939702	0.348674
0.2	0.939702	0.348674	0.2	0.926724	0.423514
0.3	1.04635	0.339858	0.3	0.912094	0.481236
0.4	1.13755	0.332581	0.4	0.895157	0.53199
0.5	1.21435	0.326257	0.5	0.874697	0.580648

Table 2: Radii of stable and unstable circular orbits. Parameters $M = 1$, $Q = 0.9$, $\Lambda = -0.6$ and $L = 3$.

The angular velocity of test particles provides a direct probe of the spacetime geometry and allows us to quantify the influence of the GB and NLED parameters on orbital motion. The angular velocity of a particle orbiting a BH, as measured by an observer at infinity and commonly referred to as the Keplerian frequency, is defined as

$$\Omega_K = \frac{d\varphi}{dt} = \frac{\dot{\varphi}}{\dot{t}} = \sqrt{\frac{\mathcal{F}(r)'}{2r}}. \quad (59)$$

The radial dependence of the Keplerian frequency for test particles orbiting the EH BH in EGB gravity is shown in Fig.12. One observes that the Keplerian frequency initially increases with the radial coordinate, reaches a maximum at an intermediate radius, and then decreases before asymptotically approaching a constant value at large distances. Furthermore, increasing the GB coupling parameter α leads to a reduction in the maximum value of the Keplerian frequency, indicating that higher-curvature corrections weaken the orbital angular velocity near the BH.

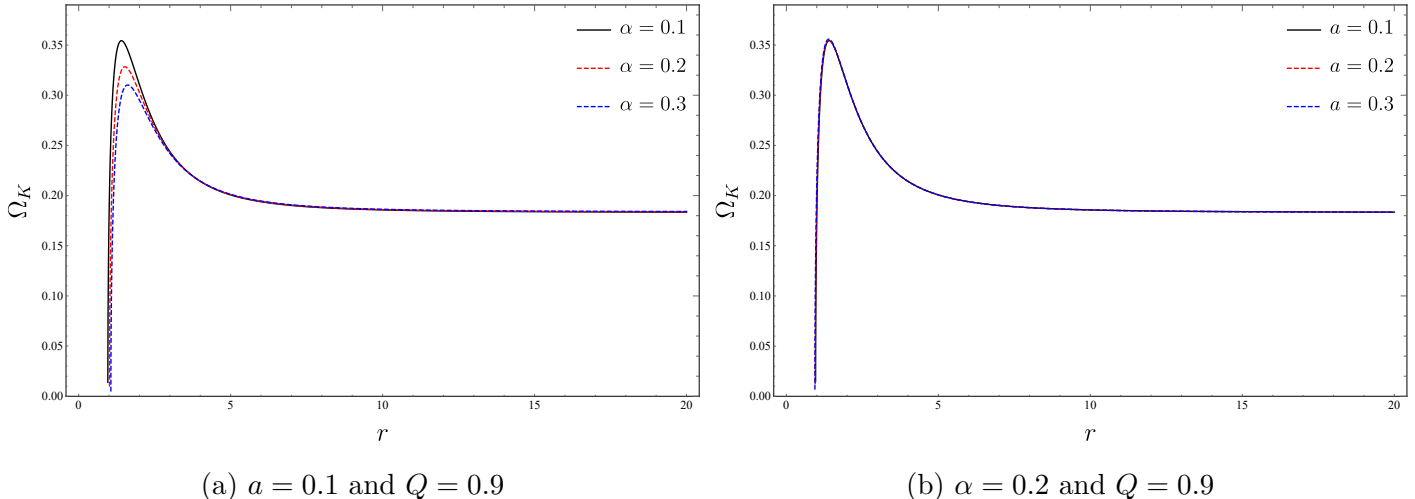


Figure 12: Keplerian frequency Ω_K for massive test particles versus r for $M = 1$ and $\Lambda = -0.1$.

To investigate the orbital dynamics of test particles, we consider small oscillations around stable circular equatorial orbits. These oscillatory motions are characterized by the radial and vertical epicyclic frequencies, which provide important information about orbital stability and the influence of spacetime curvature. The stability of circular motion in the radial and vertical directions can be analyzed through the corresponding epicyclic frequencies Ω_r and Ω_θ . From Eqs. (47) and (51), small radial and polar perturbations about a circular equatorial orbit satisfy

$$\frac{1}{2} \left(\frac{\dot{r}}{\dot{t}} \right)^2 = \frac{1}{2} \left(\frac{dr}{dt} \right)^2 = -\frac{1}{2} \frac{\mathcal{F}(r)^3}{E^2} \left[1 - \frac{E^2}{\mathcal{F}(r)} + \frac{L^2}{r^2 \sin^2 \theta} \right] \equiv V_{\text{eff}}^{(r)}, \quad (60)$$

$$\frac{1}{2} \left(\frac{\dot{\theta}}{\dot{t}} \right)^2 = \frac{1}{2} \left(\frac{d\theta}{dt} \right)^2 = \frac{1}{2} \frac{\mathcal{F}(r)^2}{r^2 E^2} \left[1 - \frac{E^2}{\mathcal{F}(r)} + \frac{L^2}{r^2 \sin^2 \theta} \right] \equiv V_{\text{eff}}^{(\theta)}, \quad (61)$$

where the $\sin \theta$ factor is retained to account for polar orbital perturbations. Introducing small deviations δr and $\delta \theta$, and differentiating Eqs. (60) and (61), with respect to the coordinate time t , we obtain

$$\frac{d^2}{dt^2} \delta r = \frac{d^2 V_{\text{eff}}^{(r)}}{dr^2} \delta r, \quad (62)$$

$$\frac{d^2}{dt^2} \delta \theta = \frac{d^2 V_{\text{eff}}^{(\theta)}}{d\theta^2} \delta \theta. \quad (63)$$

The radial and vertical epicyclic frequencies are therefore given by

$$\Omega_r^2 = \frac{d^2 V_{\text{eff}}^{(r)}}{dr^2} \quad \text{and} \quad \Omega_\theta^2 = \frac{d^2 V_{\text{eff}}^{(\theta)}}{d\theta^2}. \quad (64)$$

Combining Eqs. (56), (60) and (61), the explicit expressions for the epicyclic frequencies read

$$\Omega_r^2 = -\mathcal{F}'(r)^2 + \frac{\mathcal{F}(r)}{2r} [3\mathcal{F}'(r) + r\mathcal{F}''(r)], \quad (65)$$

$$\Omega_\theta^2 = \frac{\mathcal{F}(r)'}{2r}. \quad (66)$$

Figure 13 shows the radial profiles of the epicyclic frequencies Ω_r^2 as functions of the radial coordinate r . From Fig.13, one observes that Ω_r^2 becomes negative over a finite radial interval, indicating the presence of radially unstable circular orbits. The radial epicyclic frequency squared exhibits three zeros, separating regions of stable and unstable circular motion, with the outermost zero corresponding to the physically relevant ISCO. Furthermore, increasing GB coupling α shifts the zero of Ω_r^2 toward larger values of r implying that higher-curvature corrections enlarge the unstable region and move the ISCO outward. In contrast, increasing the EH parameter a shifts the zero of the radial epicyclic frequency toward smaller values of the radial coordinate r , indicating that NLED effects reduce the radius of the ISCO.

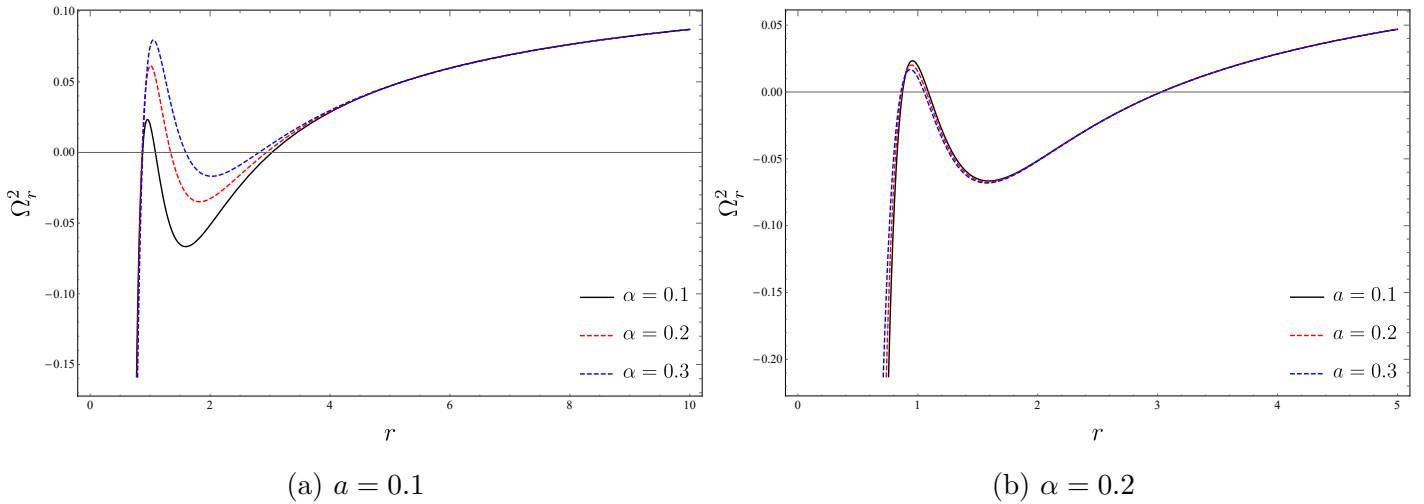


Figure 13: Radial profiles of the epicyclic frequencies Ω_r^2 versus r for $M = 1$ and $\Lambda = -0.1$.

The ISCO is of particular importance in astrophysics, as it defines the inner edge of accretion disks and sets a reference point in the inspiral phase of compact binaries, thereby influencing the emitted gravitational-wave signal and providing information about the strong-field region of the spacetime. This class of orbits is determined by the stability condition, which is given by

$$\Omega_{r_{\text{ISCO}}}^2 = 0. \quad (67)$$

Due to the complexity of the metric function, the ISCO radius is evaluated numerically for different values of the model parameters, and the results are presented in Table 3. The table shows the dependence of the ISCO parameters (r_{ISCO} , L_{ISCO} , E_{ISCO}) depend on α and a . The results indicate that the GB coupling strongly influences the ISCO, reducing the radius, angular momentum, and energy, and allowing stable orbits closer to the horizon. By contrast, variations in the EH parameter, produces only minimal changes in ISCO parameters, indicating that GB corrections dominate the orbital dynamics, while NLED effects are comparatively negligible.

$\alpha = 0.1$				$\alpha = 0.2$			
α	r_{ISCO}	L_{ISCO}	E_{ISCO}	a	r_{ISCO}	L_{ISCO}	E_{ISCO}
0.1	3.10561	5.10453	1.67953	0.1	3.02981	5.03499	1.66349
0.2	3.02981	5.03499	1.66349	0.2	3.03009	5.03526	1.66356
0.3	2.93708	4.95006	1.64376	0.3	3.03037	5.03553	1.66362
0.4	2.81557	4.84202	1.61841	0.4	3.03064	5.03581	1.66368
0.5	2.62659	4.69174	1.58259	0.5	3.03092	5.03608	1.66374

Table 3: ISCO parameters for test particles for various possible scenarios.

6 Conclusions

In this work, we have investigated charged AdS BH solutions in 4D EGB gravity coupled to EH NLED. By employing the regularized 4D EGB framework and the weak-field limit of the EH effective Lagrangian, we constructed exact BH solutions and explored the combined effects of higher-curvature corrections and nonlinear electromagnetic interactions on the geometric, thermodynamic, and dynamical properties of the spacetime. We first analyzed the horizon structure of the BH and showed that the presence of the GB coupling and the EH parameter significantly modifies the number and location of horizons. The nonlinear electromagnetic corrections introduce higher-order charge contributions, while the GB term alters the short-distance behavior of the metric, leading to notable deviations from the standard Reissner-Nordström-AdS geometry.

Within the extended phase space formalism, where the cosmological constant is interpreted as thermodynamic pressure, we examined the thermodynamic behavior of the system in detail. We derived the mass, Hawking temperature, entropy, and heat capacity, highlighting the role of the GB coupling in generating logarithmic corrections to the entropy. The thermodynamic analysis revealed the existence of critical behavior analogous to the liquid–gas phase transition, with the GB term playing a dominant role in shifting the critical point, while the EH parameter produces comparatively milder corrections. The heat capacity analysis further confirmed the presence of second-order phase transitions separating thermodynamically stable and unstable BH branches.

The JT expansion was studied by interpreting the BH mass as enthalpy, which allows us to obtain Joule Thomson coefficient, inversion temperature, and inversion pressure of an isenthalpic BH expansion. The presence of a nontrivial inversion curve indicates that BH is undergoing both heating and cooling, similar to a real thermal system. NLED effects that are described by the EH parameter a , greatly reduce the cooling region of the BH which is characterized by a low inversion temperature and pressure. Hence, these results are an indication of the non-maxwellian behavior of electrodynamics. Charged Q markedly influences the JT Effect by significantly increasing the inversion temperature and broadening the cooling region of the BH within the temperature T and pressure P coordinates. On the contrary, the GB coupling α which is associated with higher order curvature corrections, modifies the thermodynamic structure by changing the location of the inversion curve and the interplay of gravity and pressure.

Finally, we investigated the geodesic motion of test particles in the BH spacetime. The analysis of effective potentials, circular orbits, Keplerian frequencies, and orbital stability demonstrated that GB and EH corrections significantly affect particle dynamics in the strong-field regime. Higher-curvature effects tend to enlarge the region of stable circular orbits, while nonlinear electromagnetic corrections reduce it, leading to a nontrivial interplay between gravitational and electromagnetic contributions.

These results indicate that the combined effects of EGB gravity and EH NLED lead to rich and physically meaningful modifications of BH properties. This study provides further insight into the role of higher-curvature gravity and QED corrections in BH physics. Possible extensions of this work include the analysis of quasinormal modes, BH shadows, and rotating solutions within the same framework,

which may offer additional observational signatures of these corrections.

References

- [1] M. Born and L. Infeld, *Proc. R. Soc. A* **144**, 425 (1934)
- [2] B. Hoffmann, *Phys. Rev.* **47**, 877 (1935)
- [3] B. Hoffmann and L. Infeld, *Phys. Rev.* **51**, 765 (1937)
- [4] E. S. Fradkin and A. A. Tseytlin, *Phys. Lett. B* **163**, 123 (1985)
- [5] A. Garcia, H. Salazar, and J. F. Plebanski, *Nuovo Cimento B* **84**, 65 (1984)
- [6] M. Demianski, *Found. Phys.* **16**, 187 (1986)
- [7] J. Diaz-Alonso and D. Rubiera-Garcia, *Phys. Rev. D* **81**, 064021 (2010)
- [8] J. Diaz-Alonso and D. Rubiera-Garcia, *Phys. Rev. D* **82**, 085024 (2010)
- [9] H. H. Soleng, *Phys. Rev. D* **52**, 6178 (1995)
- [10] H. P. de Oliveira, *Class. Quantum Grav.* **11**, 1469 (1994)
- [11] W. Heisenberg and H. Euler, *Z. Phys.* **98**, 714 (1936)
- [12] H. Yajima and T. Tamaki, *Phys. Rev. D* **63**, 064007 (2001)
- [13] E. Ayon-Beato and A. Garcia, *Phys. Rev. Lett.* **80**, 5056 (1998)
- [14] E. Ayon-Beato and A. Garcia, *Phys. Lett. B* **464**, 25 (1999) ,
- [15] A. Burinskii and S. R. Hildebrandt, *Phys. Rev. D* **65**, 104017 (2002)
- [16] S. Shaukat, F. Javed, R. Ali, A. Waseem, F. Afandi, *Fortschr. Phys.* **73**, e70037 (2025)
- [17] B. Hamil, B.C. Lutfuoglu, *Gen. Relativ. Gravit.* **57**, 140 (2025)
- [18] B. Eslam Panah, N. Heidari, *Journal of High Energy Astrophysics* **45**, 181 (2025)
- [19] B. Eslam Panah, B. Hazarika, P. Phukon, *PTEP* **2024**, 083E02 (2024)
- [20] D. M. Yekta, M. Karimabadi, S. A. Alavi, *Annals of Physics* **434**, 168603 (2021)
- [21] D. P. Sorokin, *Fortschr. Phys.* **70**, 2200092 (2022)
- [22] M. Hassaine and C. Martinez, *Class. Quantum Grav.* **25**, 195023 (2008)
- [23] H. Maeda1, M. Hassaine, C. Martinez, *Phys. Rev. D* **79**, 044012 (2009)
- [24] A. Rincon et al., *Eur. Phys. J. C* **77**, 494 (2017)
- [25] A. Bokulic and I. Smolic, *Phys. Rev. D* **103**, 124059 (2021)
- [26] M. Dehghani, M.R. Setare, *Phys. Rev. D* **100**, 044022 (2019)
- [27] S. Habib Mazharimousavi, M. Halilsoy, *Phys. Lett. B* **681**, 190 (2009)

- [28] Z. Dayyani, A. Sheykhi, M. H. Dehghani, S. Hajkhalili, *Eur. Phys. J. C* **78**, 152 (2018)
- [29] S. Habib Mazharimousavi, *Eur. Phys. J. C* **83**, 406 (2023)
- [30] G. Arenas-Henriquez, F. Diaz, Y. Novoa, *J. High Energ. Phys.* **2023**, 72 (2023).
- [31] B. Hamil, B. C. Lutfuoglu, *Fortschr. Phys.* **73**, 2400105 (2025)
- [32] J. Schwinger, *Phys. Rev.* **82**, 664 (1951)
- [33] B. Hamil, B.C. Lutfuoglu, *Mod. Phys. Lett. A* **41**, 2550229 (2026)
- [34] H. Bouguerne, B. Hamil, B.C. Lutfuoglu, M. Merad, *Nucl. Phys. B* **1007**, 116684 (2024)
- [35] B. Hamil, L. Chetouani, *Eur. Phys. J. Plus* **131**, 311 (2016)
- [36] T. C. Adorno, S. P. Gavrilov, D.M. Gitman, *Phys. Rev. B* **110**, 014410 (2024)
- [37] I. A. Aleksandrov, G. Plunien and V. M. Shabaev, *Phys. Rev. D* **94**, 065024 (2016)
- [38] S. Biswas, A. Shaw, B. Modak, *Int. J. Mod. Phys. A* **15**, 3717 (2000)
- [39] N. Chair, M.M. Sheikh-Jabbari, *Phys. Lett. B* **504**, 141 (2001)
- [40] D. Lovelock, *J. Math. Phys.* **12**, 498 (1971)
- [41] D. Lovelock, *J. Math. Phys.* **13**, 874 (1972)
- [42] D.L. Wiltshire, *Phys. Lett. B* **169**, 36 (1986)
- [43] J.T. Wheeler, *Nucl. Phys. B* **268**, 737 (1986)
- [44] D.G. Boulware, S. Deser, *Phys. Rev. Lett.* **55**, 2656 (1985)
- [45] S.D. Odintsov, V.K. Oikonomou, *Phys. Lett. B* **805**, 135437 (2020)
- [46] S.D. Odintsov, V.K. Oikonomou, F.P. Fronimos, *Nucl. Phys. B* **958**, 115135 (2020)
- [47] D. Glavan, C. Lin, *Phys. Rev. Lett.* **124**, 081301 (2020)
- [48] Wen-Yuan Ai, *Commun. Theor. Phys.* **72**, 095402 (2020)
- [49] R. A. Hennigar, D. Kubiznak, R. B. Mann, C. Pollack, *J. High Energ. Phys.* **2020**, 27 (2020)
- [50] Fu-Wen Shu, *Phys. Lett. B* **811**, 135907 (2020)
- [51] H. Lu, Yi Pang, *Phys. Lett. B* **809**, 135717 (2020)
- [52] S. G. Ghosh, D. V. Singh, R. Kumar, S. D. Maharaj, *Annals of Physics* **424**, 168347 (2021)
- [53] N. Kumar, S. Gangopadhyay, *Gravit. Cosmol.* **30**, 149 (2024)
- [54] D. V. Singh, S. G. Ghosh, S.D. Maharaj, *Physics of the Dark Universe* **30**, 100730 (2020)
- [55] R. Kumar, S. Ul Islam, S. G. Ghosh, *Eur. Phys. J. C* **80**, 1128 (2020)
- [56] A. Biswas, *Gen. Relativ. Gravit.* **54**, 161 (2022)

- [57] H.Shah, Z. Ahmad, H. H.Shah, [Phys. Lett. B **818**, 136383 \(2021\)](#)
- [58] M. Heydari-Fard, M. Heydari-Fard, [Int. J. Mod. Phys. D **31**, 2250066 \(2022\)](#)
- [59] Y. Ladghami, B. Asfour, A. Bouali, A. Errahmani, T. Ouali, [Physics of the Dark Universe **41**, 101261 \(2023\)](#)
- [60] J. Rayimbaev, P. Tadjimuratov, B. Ahmedov, S. Palvanov, [Arab. J. Math. **11**, 119 \(2022\)](#)
- [61] A.Belhaj, Y. Sekhmani, [Gen. Relativ. Gravit. **54**, 17 \(2022\)](#)
- [62] B. Hamil, T. Birkandan, [Nucl. Phys. B **1020**, 117145 \(2025\)](#)
- [63] D. Mondal, U. Debnath, [Nucl. Phys. B **1022**, 117247 \(2026\)](#)
- [64] B. Hamil, [Int. J. Mod. Phys. A **41**, 2650017 \(2026\)](#)
- [65] Pedro G.S.Fernandes, [Phys. Lett. B **805**, 135468 \(2020\)](#)
- [66] U. Papnoi, F. Atamurotov, [Physics of the Dark Universe **35**, 100916 \(2022\)](#)
- [67] R. A. Konoplya, A. F. Zinhailo, [Eur. Phys. J. C **80**, 1049 \(2020\)](#)
- [68] P. K. Yerra, C. Bhamidipati, [Phys. Lett. B **835**, 137591 \(2022\)](#)
- [69] Shao-Wen Wei, Yu-Xiao Liu, [Phys. Rev. D **101**, 104018 \(2020\)](#)
- [70] B. Eslam Panah, K. Jafarzade, S.H. Hendi, [Nucl. Phys. B **961**, 115269 \(2020\)](#)
- [71] J.F. Plebanski, Lectures on Nonlinear Electrodynamics. (Nordita, Copenhagen 1970).
- [72] H. Salazar, A. Garcia D. and J. Plebanski, [J. Math. Phys. **28**, 2171 \(1987\)](#)
- [73] C. Lanczos, [Annals Math. **39**, 842 \(1938\)](#)
- [74] K. Jafarzade, M. K. Zangeneh, F. S. N. Lobo, [JCAP **04**, 008 \(2021\)](#)
- [75] Pedro G.S. Fernandes, [Phys.Lett B **805**, 135468 \(2020\)](#)
- [76] S. W. Hawking, [Commun.Math. Phys. **43**, 199 \(1975\)](#)
- [77] J. D. Bekenstein, [Phys. Rev. D **7**, 2333 \(1973\)](#)
- [78] D. Magos, N. Breton, [Phys. Rev. D **102**, 084011 \(2020\)](#)